ELSEVIER

Journal of Alloys and Compounds 448 (2008) 185–194

Journal of ALLOYS AND COMPOUNDS

www.elsevier.com/locate/jallcom

The Al–B–Nb–Ti system I. Re-assessment of the constituent binary systems B–Nb and B–Ti on the basis of new experimental data

V.T. Witusiewicz [a,*], A.A. Bondar [b], U. Hecht [a], S. Rex [a], T.Ya. Velikanova [b]

[a] *ACCESS e.V., Intzestr. 5, D-52072 Aachen, Germany*

[b] *Frantsevich Institute for Problems of Materials Science (IPMS), 3, Krzhyzhanivsky Street, 03680 Kiev, Ukraine*

Received 8 August 2006; received in revised form 9 October 2006; accepted 10 October 2006
Available online 30 November 2006

Abstract

Aiming to obtain a reliable description of the quaternary Al–B–Nb–Ti system, the thermodynamic descriptions of the constituent binary systems B–Nb and B–Ti are revised by modelling of the Gibbs energies of all individual phases using the CALPHAD approach and recent SGTE descriptions of the Gibbs energies of phases for pure elements. The model parameters have been evaluated taking into account the data on thermodynamic properties and phase equilibria reported in recent publications and obtained by own key measurements. The phase diagrams and the thermodynamic properties calculated with the evaluated parameters are in good agreement with the corresponding experimental data, and the thermodynamic descriptions of the systems become more suitable for high-order systems.

Keywords: B–Nb; B–Ti; Phase diagram; Thermodynamic properties; CALPHAD modelling

1. Introduction

The development of a reliable thermodynamic description of the Al–B–Nb–Ti system is of both scientific and practical importance: alloys of this system with composition (in at.%) Ti–(43–48) Al–(5–10) Nb–(0.1–1.0) B, known as niobium rich gamma-TiAl alloys, have attracted attention due to their good mechanical properties, low density and good oxidation resistance at elevated temperatures [1–4]. The addition of boron is of specific interest: it is well known that the boron alloying above 0.2 at.% lead to grain refinement of cast materials [2,5,6], however a detailed understanding of the refinement mechanism is still lacking, though several theories have been published [7,8]. Moreover, additions of boron, starting from few hundreds ppm, have been reported to refine and stabilize the lamellar structure in TiAl alloys [9], though the exact mechanism by which this is accomplished is not yet clear [10,11].

A reliable thermodynamic description of the quaternary system providing quantitative information about phase equilibria and thermodynamic properties of the multicomponent alloys is mandatory for further contributions into the problem of grain refinement and modelling of the microstructure evolution during solidification and solid state transformations.

When attempting to perform the CALPHAD modelling of the ternary Al–B–Ti and B–Nb–Ti systems based on several recent descriptions of the constituent binary B–Ti system [12–15], we observed that none of the above quoted thermodynamic descriptions of B–Ti succeeded to reproduce experimental data related to different phase equilibria with the bcc-phase based on β-Ti, the liquid and borides TiB, Ti_3B_4 and TiB_2 in the ternary systems. Concerning the thermodynamic description of the B–Nb system performed by Kaufman et al. [12] in 1984, it implied outdated phase stability data, which are incompatible with latest results. Moreover, the compound solution phases NbB and NbB_2 were modelled as stoichiometric compounds. Therefore, we performed few key experiments and re-examined the thermodynamic description of the B–Ti and B–Nb systems, taking into account more experimental data on phase equilibria, thermodynamic properties and SGTE descriptions of the Gibbs energy of phases for pure elements [16]. In the present article, part 1 we report the results on the binary B–Ti and B–Nb phase diagrams and the systems of higher order will be discussed in next parts.

* Corresponding author. Tel.: +49 241 8098007; fax: +49 241 38578.
E-mail address: victor@access.rwth-aachen.de (V.T. Witusiewicz).

0925-8388/$ – see front matter © 2006 Elsevier B.V. All rights reserved.
doi:10.1016/j.jallcom.2006.10.034

2. Thermodynamic models

2.1. Pure elements

The temperature dependence of the molar Gibbs energy of the pure elements, referred to the standard state is given by the following expression according to the Scientific Group Thermodata Europe (SGTE) [16]:

$$^{0}G - H^{\mathrm{SER}} = A + BT + CT\ln T + DT^{2} + ET^{-1} + FT^{3} + IT^{7} + JT^{-9}, \quad (1)$$

where H^{SER} is the enthalpy of a pure element at 298.15 K in its stable state (standard element reference SER). These functions for stable and metastable states of the pure elements were taken from the most recent compilation of Dinsdale [16].

2.2. Liquid phase and (β-B) solid solution

The liquid phase and the (β-B) solid solution phase in the binary B–Nb and B–Ti systems are modelled by the substitutional solution model. In the frame of this model the molar Gibbs energy (G_{m}^{ϕ}) of the phase ϕ in the B–M (M = Nb, Ti) system is expressed as

$$G_{\mathrm{m}}^{\phi}(T,x) = x_{\mathrm{B}}{}^{0}G_{\mathrm{B}}^{\phi}(T) + x_{\mathrm{M}}{}^{0}G_{\mathrm{M}}^{\phi}(T) + RT(x_{\mathrm{B}}\ln x_{\mathrm{B}} + x_{\mathrm{M}}\ln x_{\mathrm{M}}) + {}^{xs}G_{\mathrm{BM}}^{\phi}, \quad (2)$$

where R is the gas constant, T the temperature, x_i the mole fraction of component i (i = B, Ti or Nb) and $^{0}G_{i}^{\phi}$ is the molar Gibbs energy of the pure component i in phase ϕ. In Eq. (2) the summation of the first two terms on the right-hand side represents the reference part of the Gibbs energy. The next term is the ideal mixing part of the Gibbs energy and the last term ($^{xs}G_{\mathrm{BM}}^{\phi}$) represents the excess Gibbs energy being described by Redlich–Kister polynomials [17]:

$${}^{xs}G_{\mathrm{BM}}^{\phi} = x_{\mathrm{B}}x_{\mathrm{M}}\sum_{\nu=0}^{n}{}^{\nu}L_{\mathrm{B,M}}^{\phi}(x_{\mathrm{B}} - x_{\mathrm{M}})^{\nu}, \quad (3)$$

where $^{\nu}L_{\mathrm{B,M}}^{\phi}$ are the interaction parameters in the B–M system for the phase ϕ. Generally, the temperature dependence of these parameters may be expressed similar to the conventional Gibbs energy function (see Eq. (1)), but in the present work maximum two terms were applied:

$${}^{\nu}L^{\phi} = a_{\nu} + b_{\nu}T, \quad (4)$$

where a and b are parameters to be determined during the optimisation procedure.

2.3. Metal solid solution phases (bcc-Nb), (bcc-Ti) and (hcp-Ti)

Analogous to the binary system B–Ti [15], the solution phases (bcc-Nb), (bcc-Ti) and (hcp-Ti) were described with the two-sublattice model developed by Hillert and Staffansson [18], considering solid solubility of B in the metal phases as interstitial. The two sublattices being expressed by the general formula $(\mathrm{M})_1(\mathrm{B,Va\%})_a$. Here Va denotes the amount of vacancies and % designates the major component in the related sublattice. The subscript a is the number of interstitial sites per metal (M) atom, which is equal to 3 for (bcc-Ti) and (bcc-Nb) and 0.5 for (hcp-Ti). In detail the equation for molar Gibbs energy for this model is given elsewhere [15,19–21].

2.4. Boride solution phases NbB, TiB, NbB_2 and TiB_2

For the description of the molar Gibbs energy of monoborides and diborides the two-sublattice models $(\mathrm{M})_1(\mathrm{B\%,M})_1$ and $(\mathrm{B,M\%})_1(\mathrm{B\%,M})_2$ are adapted from the description of B–Ti system [15], respectively, where M denotes Nb or Ti and % designates the major component in the related sublattice.

2.5. Boride stoichiometric phases Nb_3B_2, Nb_5B_6, Nb_3B_4, Nb_2B_3 and Ti_3B_4

The sublattice model by Hillert and Staffansson [18] allows also describe stoichiometric phases. In this case each sublattice is occupied by only one kind of atoms and the molar Gibbs energy of binary stoichiometric borides simplifies to

$$G_{\mathrm{M}:\mathrm{B}}^{\mathrm{M}_i\mathrm{B}_j}(T) - iH_{\mathrm{M}}^{\mathrm{SER}}(298.15\,\mathrm{K}) - jH_{\mathrm{B}}^{\mathrm{SER}}(298.15\,\mathrm{K}) = i^{0}G_{\mathrm{M}}^{\phi}(T) + j^{0}G_{\mathrm{B}}^{\beta}(T) + a^{\mathrm{M}_i\mathrm{B}_j} + b^{\mathrm{M}_i\mathrm{B}_j}T + c^{\mathrm{M}_i\mathrm{B}_j}T\ln T + d^{\mathrm{M}_i\mathrm{B}_j}T^{2} + e^{\mathrm{M}_i\mathrm{B}_j}T^{-1} + f^{\mathrm{M}_i\mathrm{B}_j}T^{3} + \ldots, \quad (5)$$

where the $^{0}G_{\mathrm{B}}^{\beta}(T)$ and $^{0}G_{\mathrm{M}}^{\phi}(T)$ represents the molar Gibbs energy of (β-B), Nb (bcc) or Ti (hcp), respectively, and a, b, c, ... are optimisation parameters.

3. Experimental and assessed data used for modelling

3.1. The binary system B–Nb

The most complete and reliable phase diagram for the binary B–Nb system constructed on the basis of accurate experimental investigations is the diagram published in [22]. This phase diagram was adopted by Rogl [23,24] for constructing ternary systems. In well-known handbooks [25] and [26] the phase diagram of the B–Nb system is presented on the basis of experimental data of [27] and [28], respectively. In [27] there are data only for the range 0 to ~20 at.% B, and the work of [28] is less reliable and precise due to contaminated samples, as shown in more recent publications [22,23,27, etc.]. Therefore, in the present work we have used the phase diagram of [22], as it was selected also in the monographs [23,24]. Minor modifications have been introduced to account for experimental data on the solubility of B in Nb, on the recently identified borides Nb_5B_6 and Nb_2B_3 as well as on the co-ordinates of the (Nb) + NbB eutectic, as described below.

The solubility of B in Nb was measured by Zakharov and Pshokin [27,29,30] at several temperatures. These data, reproduced in Table 1, somewhat differ from source to source, nevertheless both these series were used in the present optimisation. In the same papers the co-ordinates of the invariant eutectic point for the reaction $L \rightarrow$ (Nb) + NbB were found to be 1.6 wt.% B (12 at.%) and 2443 ± 20 K. The given temperature corresponds well to the value of [22] (2438 ± 13 K) if taking into account the difference between the International Practical Temperature Scales IPTS-48 and IPTS-68, but it deviates strongly from ~1873 K in [28]. In the same time, the composition of the eutectic from [27,29,30] (12 at.% B) differs significantly from [22] (19 ± 2 at.% B) and [28]

Table 1
Solubility of B in solid Nb

T (K)	Solubility		Reference
	wt.% B	at.% B	
2443 ± 20 (melting)	0.35	2.9	[27]
	0.23	1.9	[29,30]
2223	0.26	2.2	[27]
	0.16	1.4	[29,30]
1873	0.15	1.3	[27]
	0.09	0.8	[29,30]
1473	0.05	0.4	[27]
	0.03	0.3	[29,30]

(20 at.% B). Recently, Borges et al. [31] as well as Borysov et al. [32] have performed microstructure investigations of B–Nb alloys and reported the composition of the eutectic to be 16 and 15 at.% B, respectively. Borysov et al. reported the eutectic temperature to be 2463 ± 13 K [32], based on pyrometric measurements. For this key experiment in [32] the Nb–B alloys were prepared by arc melting with a non-consumable tungsten electrode on a water-cooled copper hearth under purified argon. The initial materials were bar Nb (99.8 wt.% Nb) and amorphous boron. The original B powder contained 5.3% O, 0.55% H, <0.005% N, 10^{-1}% Cu, <10^{-2}% Fe and <10^{-2}% Si (in wt.%) and therefore it was previously melted alone in an arc furnace for purification followed by crushing to small pieces. The purification was quite effective so that oxygen content was 0.06 wt.% in the alloy Nb–14 at.% B, and N and H contents were lower of threshold of sensitivity about 10^{-3} wt.%. The composition of the alloy was checked by wet chemical analysis. The pyrometer EOP-66 was calibrated in the Ukrainian National Metrological Laboratory and the technique was similar to [22].

The homogeneity range of the boride NbB is rather small and does not exceed 2 at.% with a maximum that corresponds to the congruent melting point at 50 at.% B and 3194 ± 13 K [22].

In the phase diagram of [22] the Nb_5B_6 boride is absent, though it was found to be easily obtained by arc melting [33]. Thus, it is highly probable that this boride occurs through a peritectic reaction of liquid and Nb_3B_4, further participating in formation of the eutectic with NbB according to the reaction $L \leftrightarrow NbB + Nb_5B_6$. Such sequence of equilibria is common also to the analogous B–V system [34]. It seems to be quite probable that the borides Nb_5B_6 and Nb_3B_4 are stoichiometric, though in the phase diagram of [22] the boride Nb_3B_4 has a considerable homogeneity ranges, based on phase constituents determined for an alloy annealed at 2973 K. These data could be untrustworthy, taking proper account of difficulties of accurate composition control in the high-temperature region and the fact that in [22] the problem of identification of Nb_5B_6 was not solved.

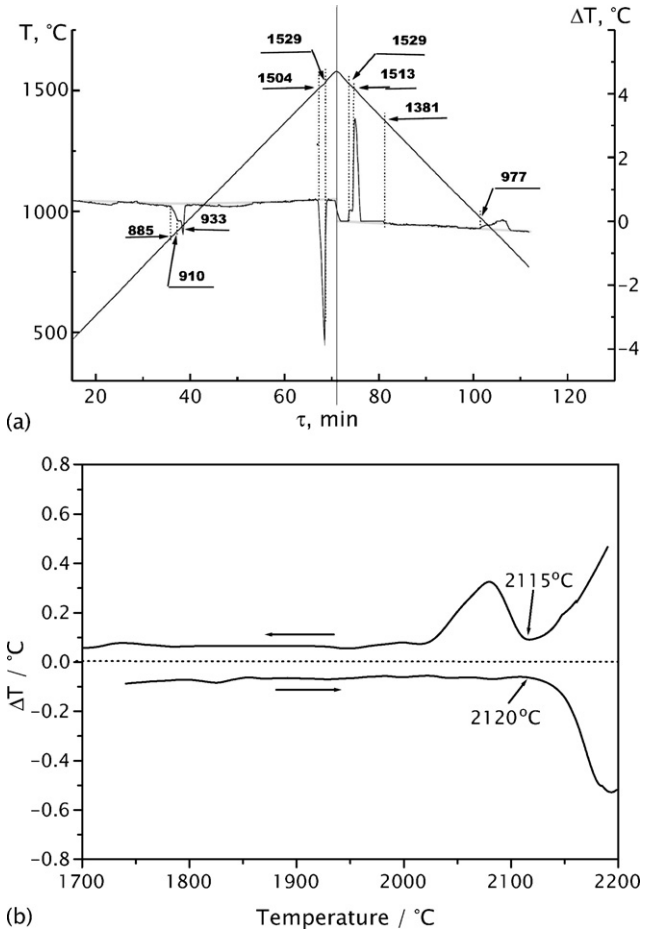

Fig. 1. The DTA curves upon heating and cooling with rate 20 K min^{-1} using yttria crucible of the binary as-cast Ti–7.0 at.% B (a) and annealed at 2373 K Ti–55 at.% B (b) alloys.

There is no doubt that the NbB_2 boride has a rather large homogeneity range. According to [22] this range extends from ∼61 up to ∼70 at.% B with the congruent melting point at the composition $Nb_{34}B_{66}$. Recently, Nunes et al. [35] have evaluated the homogeneity range of the NbB_2-phase by detailed microstructural characterisation of as-cast, as-cast + annealed and solid state

Table 2
Crystal structure data for the B–Nb and B–Ti solid phases [13,15,23–26,48] and their modelling

Phase	Prototype	Pearson symbol	Space group	Structurbericht designation	Model applied
Nb (bcc-Nb), β-Ti (bcc-Ti)	W	*cI*2	$Im\bar{3}m$	*A*2	$[(M)_1: (B,Va\%)_3]$[a]
α-Ti (hcp-Ti)	Mg	*hP*2	$P6_3/mmc$	*A*3	$[(Ti)_1: (B,Va\%)_{0.5}]$
β-B	β-B	*hR*108	$R\bar{3}m$	–	[B%,M]
Nb_3B_2	U_3Si_2	*tP*10	*P*4/*mbm*	$D5_a$	$[(Nb)_3: (B)_2]$
NbB	CrB	*oC*8	*Cmcm*	B_f	$[(Nb)_1: (B\%,Nb)_1]$
TiB	FeB	*oP*8	*Pnma*	*B*27	$[(Ti)_1: (B\%,Ti)_1]$
NbB_2, TiB_2	AlB_2	*hP*3	*P*6/*mmm*	*C*32	$[(B,M\%)_1: (B\%,M)_2]$
Nb_5B_6	V_5B_6	*oC*22	*Cmmm*	–	$[(Nb)_5: (B)_6]$
Nb_3B_4, Ti_3B_4	Ta_3B_4	*o*/14	*Immm*	$D7_b$	$[(M)_3: (B)_4]$
Nb_2B_3	V_2B_3	*oC*20	*Cmcm*	–	$[(Nb)_2: (B)_3]$

[a] M denotes Nb or Ti.

Table 3
Summary of thermodynamic parameters for the phases in the binary system B–Nb

Phase	Parameters (J mol^{-1})
Liquid	${}^0L^{\mathrm{Liq}}_{\mathrm{B,Nb}} = -182227 + 5.092T$; ${}^1L^{\mathrm{Liq}}_{\mathrm{B,Nb}} = 13667 - 27.617T$; ${}^2L^{\mathrm{Liq}}_{\mathrm{B,Nb}} = 8815$
β-B	${}^0G^{\beta}_{\mathrm{Nb}} - H^{\mathrm{SER}}_{\mathrm{Nb}} = 10000 + {}^0GH^{\mathrm{SER}}_{\mathrm{Nb}}$; ${}^0L^{\beta}_{\mathrm{B,Nb}} = -150535$
bcc_A2 (Nb)	${}^0G^{\mathrm{BCC}}_{\mathrm{Nb:B}} - H^{\mathrm{SER}}_{\mathrm{Nb}} - 3H^{\mathrm{SER}}_{\mathrm{B}} = {}^0GH^{\mathrm{SER}}_{\mathrm{Nb}} + 3{}^0GH^{\mathrm{BCC}}_{\mathrm{B}} - 321703 + 125.621T$; ${}^0G^{\mathrm{BCC}}_{\mathrm{Nb:Va}} - H^{\mathrm{SER}}_{\mathrm{Nb}} = {}^0GH^{\mathrm{SER}}_{\mathrm{Nb}}$; ${}^0L^{\mathrm{BCC}}_{\mathrm{Nb:B,Va}} = -167421$
NbB	${}^0G^{\mathrm{NbB}}_{\mathrm{Nb:Nb}} - 2H^{\mathrm{SER}}_{\mathrm{Nb}} = 75000 + 2{}^0GH^{\mathrm{SER}}_{\mathrm{Nb}}$; ${}^0G^{\mathrm{NbB}}_{\mathrm{Nb:B}} - H^{\mathrm{SER}}_{\mathrm{B}} - H^{\mathrm{SER}}_{\mathrm{Nb}} =$ ${}^0GH^{\mathrm{SER}}_{\mathrm{B}} + {}^0GH^{\mathrm{SER}}_{\mathrm{Nb}} - 157380 - 21.8\,\mathrm{T} + 3.381T\ln(T) - 1.953\times10^{-4}T^2$
Nb_3B_2	${}^0G^{\mathrm{Nb_3B_2}}_{\mathrm{Nb:B}} - 2H^{\mathrm{SER}}_{\mathrm{B}} - 3H^{\mathrm{SER}}_{\mathrm{Nb}} = 2{}^0GH^{\mathrm{SER}}_{\mathrm{B}} + 3{}^0GH^{\mathrm{SER}}_{\mathrm{Nb}} - 372301 - 53.233T + 11.662T\ln(T) - 2.276\times10^{-3}T^2$
Nb_5B_6	${}^0G^{\mathrm{Nb_5B_6}}_{\mathrm{Nb:B}} - 6H^{\mathrm{SER}}_{\mathrm{B}} - 5H^{\mathrm{SER}}_{\mathrm{Nb}} = 6{}^0GH^{\mathrm{SER}}_{\mathrm{B}} + 5{}^0GH^{\mathrm{SER}}_{\mathrm{Nb}} - 886400 - 87.40T + 13.75T\ln(T) + 8.756\times10^{-4}T^2$
Nb_3B_4	${}^0G^{\mathrm{Nb_3B_4}}_{\mathrm{Nb:B}} - 4H^{\mathrm{SER}}_{\mathrm{B}} - 3H^{\mathrm{SER}}_{\mathrm{Nb}} = 4{}^0GH^{\mathrm{SER}}_{\mathrm{B}} + 3{}^0GH^{\mathrm{SER}}_{\mathrm{Nb}} - 571700 - 35.515T + 5.807T\ln(T) + 1.671\times10^{-3}T^2$
Nb_2B_3	${}^0G^{\mathrm{Nb_2B_3}}_{\mathrm{Nb:B}} - 3H^{\mathrm{SER}}_{\mathrm{B}} - 2H^{\mathrm{SER}}_{\mathrm{Nb}} = 3{}^0GH^{\mathrm{SER}}_{\mathrm{B}} + 2{}^0GH^{\mathrm{SER}}_{\mathrm{Nb}} - 412500 - 39.85T + 6.25T\ln(T) + 3.98\times10^{-4}T^2$
NbB_2	${}^0G^{\mathrm{NbB_2}}_{\mathrm{B:B}} - 3H^{\mathrm{SER}}_{\mathrm{B}} = 89628 + 3{}^0GH^{\mathrm{SER}}_{\mathrm{B}}$; ${}^0G^{\mathrm{NbB_2}}_{\mathrm{Nb:Nb}} - 3H^{\mathrm{SER}}_{\mathrm{Nb}} = 75000 + 3{}^0GH^{\mathrm{SER}}_{\mathrm{Nb}}$; ${}^0G^{\mathrm{NbB_2}}_{\mathrm{Nb:B}} - 2H^{\mathrm{SER}}_{\mathrm{B}} - H^{\mathrm{SER}}_{\mathrm{Nb}} =$ $2{}^0GH^{\mathrm{SER}}_{\mathrm{B}} + {}^0GH^{\mathrm{SER}}_{\mathrm{Nb}} - 253125 + 25.7T - 3.268T\ln(T) + 2.746\times10^{-3}T^2$; ${}^0G^{\mathrm{NbB_2}}_{\mathrm{B:Nb}} - H^{\mathrm{SER}}_{\mathrm{B}} - 2H^{\mathrm{SER}}_{\mathrm{Nb}} =$ ${}^0GH^{\mathrm{SER}}_{\mathrm{B}} + 2{}^0GH^{\mathrm{SER}}_{\mathrm{Nb}}$; ${}^0L^{\mathrm{NbB_2}}_{\mathrm{B,Nb:B}} = {}^0L^{\mathrm{B_2Nb}}_{\mathrm{Nb:B,Nb}} = -110590 + 22.072T$; ${}^0L^{\mathrm{NbB_2}}_{\mathrm{B:B,Nb}} = {}^0L^{\mathrm{B_2Nb}}_{\mathrm{B,Nb:Nb}} = -205000 + 25.771T$

All values are given in SI units (J, mol, K) and for 1 mol of formula unit.

sintered B–Nb alloys. The neutron diffraction experiment clearly showed that the width of the homogeneity range of this phase is nearly 5 at.% extending from 65 up to 70 at.% B at 2073 K.

Between Nb_3B_4 and NbB_2 there exists one more stoichiometric boride Nb_2B_3 that was synthesised in Cu melt at 1973 K [36]. It is unknown yet up to what temperature this boride is stable. Thus, the authors of [33] have reported that in as-cast alloys with composition Nb–60 at.% B this boride was not found. This may indicate that Nb_2B_3 forms according to peritectoid reaction from Nb_3B_4 and NbB_2.

Crespo et al. [37] found a small increase of unit cell volume by 3.2×10^6 pm^3 for the β-B-based phase saturated by Nb at 2223 K for 24 h and explained this fact by dissolving of ~0.1 at.% Nb.

Concerning the thermodynamic properties of B–Nb alloys, the majority of experimental investigations deal with determination of the enthalpy change of different borides upon heating [38,39]. Using these data the heat capacity of Nb_3B_2, Nb_3B_4, $NbB_{0.99}$ and $NbB_{1.96}$ borides were evaluated as a function of temperature [39,40].

Numerous publications on the standard enthalpy of formation of non-stoichiometric diboride NbB_2 can be found [41–47]. The data of [41,42,44] agree well with one another, while the values reported in the other articles are less negative and scatter strongly. Due to this, in the present optimisation the data of [41,42,44] were used with twice as high confidence factor than the others.

3.2. The binary system B–Ti

Thermodynamic descriptions of the B–Ti system have been reported earlier by Kaufman et al. [12], Murray et al. [13], Bätzner [14] and Ma et al. [15]. The assessments of [12] and [13] have incorporated old Gibbs energy data for pure elements and are no longer useful in combination with new reference data for pure elements from Dinsdale [16] used for the higher order systems. The description of Bätzner [14] treated the compound solution phases TiB and TiB_2 as stoichiometric compounds, though homogeneity ranges 49–50 at.% B [51] and 65.2–67.6 at.% B [22,49] were experimentally observed for TiB and TiB_2, respectively. In the most recent thermodynamic description of Ma et al. [15], which is based on the same experimental data as [13], these solubility ranges were modelled using the two-sublattice model. Unfortunately, the composition and the temperature ranges of two-phase equilibria between liquid, β-Ti and boride phases are modelled such that the majority of recent experimental data in the ternary Al–B–Ti system [50] could not be well reproduced.

Firstly, to prove the composition and temperature of the eutectic in the Ti-rich corner, few DTA-experiments with alloys containing 7.0, 55 and 61 at.% B were performed in the present work as to complement earlier measurements of two other binary alloys, i.e. Ti–5 at.% B and Ti–7.5 at.% B [32,50]. The alloys were prepared by arc melting from iodide titanium (99.9 wt.% Ti) and amor-

Table 4
Summary of thermodynamic parameters for the phases in the binary system B–Ti

Phase	Parameters (J mol^{-1})
Liquid	${}^0L^{\mathrm{Liq}}_{\mathrm{B,Ti}} = -240892 + 13.510T$; ${}^1L^{\mathrm{Liq}}_{\mathrm{B,Ti}} = -33241 - 21.867T$; ${}^2L^{\mathrm{Liq}}_{\mathrm{B,Ti}} = 42976 + 3.875T$; ${}^3L^{\mathrm{Liq}}_{\mathrm{B,Ti}} = 38759$;
β-B	${}^0G^{\beta}_{\mathrm{Ti}} - H^{\mathrm{SER}}_{\mathrm{Ti}} = 10000 + {}^0GH^{\mathrm{SER}}_{\mathrm{Ti}}$
bcc_A2 (β-Ti)	${}^0G^{\mathrm{BCC}}_{\mathrm{Ti:B}} - H^{\mathrm{SER}}_{\mathrm{Ti}} - 3H^{\mathrm{SER}}_{\mathrm{B}} = {}^0GH^{\mathrm{BCC}}_{\mathrm{Ti}} + 3{}^0GH^{\mathrm{BCC}}_{\mathrm{B}} - 239999$; ${}^0G^{\mathrm{BCC}}_{\mathrm{Ti:Va}} - H^{\mathrm{SER}}_{\mathrm{Ti}} = {}^0GH^{\mathrm{BCC}}_{\mathrm{Ti}}$; ${}^0L^{\mathrm{BCC}}_{\mathrm{Ti:B,Va}} = -14723$
hcp_A3 (α-Ti)	${}^0G^{\mathrm{HCP}}_{\mathrm{Ti:B}} - H^{\mathrm{SER}}_{\mathrm{Ti}} - 0.5H^{\mathrm{SER}}_{\mathrm{B}} = {}^0GH^{\mathrm{SER}}_{\mathrm{Ti}} + 0.5{}^0GH^{\mathrm{SER}}_{\mathrm{B}} - 56229$; ${}^0G^{\mathrm{HCP}}_{\mathrm{Ti:Va}} - H^{\mathrm{SER}}_{\mathrm{Ti}} = {}^0GH^{\mathrm{SER}}_{\mathrm{Ti}}$; ${}^0L^{\mathrm{HCP}}_{\mathrm{Ti:B,Va}} = 9115$;
TiB	${}^0G^{\mathrm{TiB}}_{\mathrm{Ti:Ti}} - 2H^{\mathrm{SER}}_{\mathrm{Ti}} = 40000 + 2{}^0GH^{\mathrm{SER}}_{\mathrm{Ti}}$; ${}^0G^{\mathrm{TiB}}_{\mathrm{Ti:B}} - H^{\mathrm{SER}}_{\mathrm{B}} - H^{\mathrm{SER}}_{\mathrm{Ti}} =$ ${}^0GH^{\mathrm{SER}}_{\mathrm{B}} + {}^0GH^{\mathrm{SER}}_{\mathrm{Ti}} - 165000 - 67.317T + 9.5T\ln(T) - 5.0\times10^{-4}T^2$; ${}^0L^{\mathrm{TiB}}_{\mathrm{Ti:B,Ti}} = -37503 + 29.790T$;
Ti_3B_4	${}^0G^{\mathrm{Ti_3B_4}}_{\mathrm{Ti:B}} - 4H^{\mathrm{SER}}_{\mathrm{B}} - 3H^{\mathrm{SER}}_{\mathrm{Ti}} = 4{}^0GH^{\mathrm{SER}}_{\mathrm{B}} + 3{}^0GH^{\mathrm{SER}}_{\mathrm{Ti}} - 660000 - 162.241T + 25.0T\ln(T) - 2.0\times10^{-3}T^2$
TiB_2	${}^0G^{\mathrm{TiB_2}}_{\mathrm{B:B}} - 3H^{\mathrm{SER}}_{\mathrm{B}} = +89628 + 3{}^0GH^{\mathrm{SER}}_{\mathrm{B}}$; ${}^0G^{\mathrm{B_2Ti}}_{\mathrm{Ti:Ti}} - 3H^{\mathrm{SER}}_{\mathrm{Ti}} = 18000 + 3{}^0GH^{\mathrm{SER}}_{\mathrm{Ti}}$; ${}^0G^{\mathrm{TiB_2}}_{\mathrm{Ti:B}} - 2H^{\mathrm{SER}}_{\mathrm{B}} - H^{\mathrm{SER}}_{\mathrm{Ti}} =$ $2{}^0GH^{\mathrm{SER}}_{\mathrm{B}} + {}^0GH^{\mathrm{SER}}_{\mathrm{Ti}} - 329000 + 1.865T + 1.2547T\ln(T) + 3.131\times10^{-3}T^2 - 4.105\times10^{-7}T^3$; ${}^0G^{\mathrm{TiB_2}}_{\mathrm{B:Ti}} - H^{\mathrm{SER}}_{\mathrm{B}} - 2H^{\mathrm{SER}}_{\mathrm{Ti}} =$ ${}^0GH^{\mathrm{SER}}_{\mathrm{B}} + 2{}^0GH^{\mathrm{SER}}_{\mathrm{Ti}}$; ${}^0L^{\mathrm{TiB_2}}_{\mathrm{B,Ti:B}} = {}^0L^{\mathrm{TiB_2}}_{\mathrm{B,Ti:Ti}} = -91514 + 46.777T$; ${}^0L^{\mathrm{TiB_2}}_{\mathrm{B:B,Ti}} = {}^0L^{\mathrm{B_2Ti}}_{\mathrm{Ti:B,Ti}} = -18500 + 53.211T$

All values are given in SI units (J, mol, K) and for 1 mol of formula unit.

phous boron. Oxygen content was about 0.1 wt.%, and N and H contents were lower than the threshold of sensitivity, e.g. about 10^{-3} wt.% for the Ti–7.0 at.% B alloy. Alloy composition was checked by wet chemical analysis for B. The DTA apparatus was calibrated using secondary reference points of IPTS-90 together with high purity Fe and (Mo) + Mo_2C eutectic. It showed reproducibility of all transformation temperatures to be not worse than ∼1%. The DTA curve obtained for the Ti–7.0 at.% B alloy upon heating and cooling in an yttria crucible is shown in Fig. 1a. Temperatures of transformation were assumed to correspond to the onset temperature of departure from the DTA base-line. The results of this experiment as well as those obtained for other Ti–B samples [32,50] showed that the composition and the temperature of the eutectic is 7.0–7.5 at.% B and 1777 K, respectively. Thus, the composition of the eutectic well agrees with the data of [13,22], but the temperature of the eutectic reaction is 36 K lower than measured by Rudy [22] and assessed by Murray et al. [13].

Secondly, it was necessary to check the temperature of the peritectic reactions $L + Ti_3B_4 \leftrightarrow TiB$ and $L + TiB_2 \leftrightarrow Ti_3B_4$, because available literature data are contradictory: in the assessments [13–15] these reactions were assigned 2453 and 2473 K, respectively, being close to Rudy [22] who reported the reaction $L + TiB_2 \leftrightarrow TiB$ at 2463 ± 20 K. In the publications [51,52] the reaction $L + Ti_3B_4 \leftrightarrow TiB$ is assigned a temperature of 2273 ± 50 K and in [53] of ∼2333 K. To verify temperatures of these reactions few key experiments with binary Ti–55 at.% B and Ti–61 at.% alloys B were performed by XRD and thermal analysis in the frame of this work. The samples were prepared by arc melting using the same materials and procedures as described above. Oxygen content was about 0.02 wt.%. Nitrogen and hydrogen contents as in previous cases were lower than the threshold of sensitivity. One piece of each alloy was annealed for 1 h in argon gettered by Ta at 2373 K. The XRD analyses (a DRON-3M diffractometer used Cu Kα filtered radiation) of the as-cast as well as the annealed samples show that they contained all the three borides (TiB, Ti_3B_4 and TiB_2) and that the performed annealing increased the Ti_3B_4 content. As an example the DTA curves obtained upon heating and cooling for the annealed Ti–55 at.% B sample are shown in Fig. 1b. The DTA shows the initial melting temperature to be 2393 K, while the pyrometric Pirani–Altertum method gave 2428 ± 25 K that is close to the value reported by Rudy [22]. The DTA temperature is hereafter treated as relating to the reaction $L + Ti_3B_4 \leftrightarrow TiB$, and the pyrometric temperature seems to be rather overestimated owing to small quantity of liquid and to be close to the next reaction $L + TiB_2 \leftrightarrow Ti_3B_4$. All other phase equilibria as well as thermodynamic properties used for the present optimisation were the same as selected by [15].

Table 5
Invariant reactions in the B–Nb system[a]

Reaction between phases $\phi_1/\phi_2/\phi_3$	Type	T (K)	Content of B in phases (at.%)			Comment/Reference
			ϕ_1	ϕ_2	ϕ_3	
$L \leftrightarrow bcc + Nb_3B_2$	Eutectic	∼1873	20	∼3[b]	∼40[b]	Experiment [28]
$L \leftrightarrow bcc + NbB$	Eutectic	**2441 ± 12**[c]	**19 ± 2**	∼2	∼49	Experiment [22]
		2443 ± 20	**12**	–	–	Experiment [27,29,30]
		2463 ± 13	**15**	–	–	Experiment [this work]
		2439	15.1	0.5	50.0	Assessment [12]
		2453	15.1	2.0	48.8	This assessment
$L + NbB \leftrightarrow Nb_3B_2$	Peritectic	∼2113[b]	38.5[b]	∼50[b]	∼40[b]	Experiment [28]
$bcc + NbB \leftrightarrow Nb_3B_2$	Peritectoid	**2353 ± 40**	**∼0.9**[b]	**∼50**	**∼40**	Experiment [22]
		2209	0.3	50.0	40.0	Assessment [12]
		2350	1.9	49.0	40.0	This assessment
$L \leftrightarrow NbB$	Congruent	∼2563[b]	50	50	–	Experiment [28]
		3194 ± 13[c]	**∼50**	**∼50**	–	Experiment [22]
		3176	49.9	49.9	–	This assessment
$L \leftrightarrow NbB + Nb_3B_4$	Eutectic	∼3023[b]	∼53[b]	∼50[b]	∼57[b]	Experiment [28]
		3137 ± 17[c]	**54**	**∼51**[b]	**∼57.5**[b]	Experiment [22]
		3044	58.2	50.0	57.1	Assessment [12]
$L \leftrightarrow NbB + Nb_5B_6$	Eutectic	3174.1	51.4	49.9	54.5	This assessment
$L + Nb_3B_4 \leftrightarrow Nb_5B_6$	Peritectic	3174.2	51.4	57.1	54.5	This assessment
$L + NbB_2 \leftrightarrow Nb_3B_4$	Peritectic	**∼2993**[b]	**55.5**[b]	**∼64**[b]	**∼57**[b]	Experiment [28]
		3212 ± 14[c]	**57.3**[b]	**∼61**[b]	**∼58**[b]	Experiment [22]
		3169	58.2	70.0	57.1	Assessment [12]
		3186	52.7	61.0	57.1	This assessment
$? \leftrightarrow Nb_2B_3$	?	**>1973**	–	–	–	Experiment [36]
$Nb_3B_4 + NbB_2 \leftrightarrow Nb_2B_3$	Peritectoid	2650	57.1	65.9	60.0	This assessment
$L \leftrightarrow NbB_2$	Congruent	3273	66.6	66.6	–	Experiment [28]
		3313 ± 18[c]	**66**	**66**	–	Experiment [22]
		3308	66.7	66.7	–	Assessment [12]
		3303	65.9	65.9	–	This assessment
$L \leftrightarrow NbB_2 + (\beta B)$	Eutectic	**∼2213**[b]	**∼91**[b]	**∼74**[b]	**∼97.5**[b]	Experiment [28]
		2310 ± 22[c]	**∼98**	**∼70**[b]	**∼99.5**[b]	Experiment [22]
		2234	95.8	70.0	100	Assessment [12]
		2285	95.4	70.3	99.5	This assessment

[a] The data printed in bold letters are those used for the optimisation.
[b] Taken from Figure.
[c] Corrected for differences between IPTS-48 and IPTS-90.

3.3. Crystal structure

The crystal structures of the phases in the binary B–Nb and B–Ti systems and the models used for the description of these phases are summarized in Table 2. Nb and β-Ti, diborides NbB_2 and TiB_2 as well as borides Nb_3B_4 and Ti_3B_4 are isostructural phases, respectively. Due to this all isostructural phases were modelled using analogous models (see Sections 2.4 and 2.5). This allows simple integration of these models in a thermodynamic description of higher order systems.

4. Optimisation

The parameters of the thermodynamic models that were evaluated in the present work are the interaction parameters of all individual phases in the B–Nb and B–Ti systems. The model parameters were evaluated by searching for the best fit to the experimental phase equilibrium data and thermodynamic data using the PARROT optimiser of the Thermo-Calc software [20]. The PARROT can handle various kinds of experimental data minimizing an error sum where each of the selected experimental values is given a certain weight. The weight is chosen by personal judgement and changed by trial and error during the work until most of the selected experimental data were reproduced within the expected uncertainly limits.

The optimisation in both systems started with those borides, for which the data on the heat capacity or enthalpy changes upon heating were available. Thus, the values of the parameters labelled c, d, e and f (see Eq. (5)) for the borides were derived by best fitting of these experimental values setting the weight equal to zero for all other experimental phase equilibria and thermody-

Table 6
Invariant reactions in the B–Ti system[a]

Reaction between phases $\phi_1/\phi_2/\phi_3$	Type	T (K)	Content of B in phases (at.%)			Comment/reference
			ϕ_1	ϕ_2	ϕ_3	
bcc + TiB ↔ hcp	Peritectoid	**1159 ± 4**	**<0.2**	–	–	Experiment [53]
			<1.7		**∼0.1**	Experiment [70]
		1158	–	–	–	Experiment [this work]
		1156	0.05	48.3	0.09	Assessment [15]
		1156	0.01	48.9	0.03	This assessment
$L + TiB_2 \leftrightarrow TiB$	Peritectic	2463 ± 20	–	–	–	Experiment [22]
$L + TiB_2 \leftrightarrow Ti_3B_4$	Peritectic	**2293**	–	–	–	Experiment [51]
		2473 ± 25	**42 ± 3**	**∼65.5**	**58.1**	Assessment [13]
		2477	41.9	65.0	57.1	Assessment [15]
		2414	31.7	65.9	57.1	This assessment
$L + Ti_3B_4 \leftrightarrow TiB$	Peritectic	**2333**	–	–	–	Experiment [70]
		2174 ± 50	–	–	–	Experiment [52]
		–	–	–	**49.3**	Experiment [49]
		2273	–	**57.14**	–	Experiment [51]
		2393	–	–	–	Experiment [this work]
		2453	∼39	58.1	50.0	Assessment [13]
		2453	41.3	57.1	50.0	Assessment [15]
		2390	30.9	57.1	49.7	This assessment
$L \leftrightarrow TiB_2$	Congruent	>3153	–	67	–	Experiment [51]
		3498 ± 25	–	**66.3**	–	Experiment [22]
		3123 ± 50	–	–	–	Experiment [67]
		3173 ± 70	–	–	–	Experiment [68]
		3063 ± 30	–	–	–	Experiment [66]
		3193	–	–	–	Experiment [52,69]
		3498	–	–	–	Experiment [65]
		3498 ± 25	**66.7**	**66.7**	—	Assessment [13]
		3498	66.7	66.7	–	Assessment [15]
		3476	66.7	66.7	–	This assessment
$L \leftrightarrow TiB_2 + (\beta\text{-B})$	Eutectic	**2353 ± 20**	**>98**	–	–	Experiment [22]
		2353 ± 20	**∼98**	**∼66.7**	**∼100**	Assessment [13]
		2330	97.5	67.6	100	Assessment [15]
		2334	98.5	66.8	100	This assessment
$L \leftrightarrow$ bcc + TiB	Eutectic	1813 ± 10	**7 ± 1**	–	–	Experiment [22]
		1803 ± 10	>1	–	–	Experiment [51]
		∼1943	–	–	–	Experiment [53]
		1777	–	–	–	Experiment [this work]
		1813 ± 10	**7 ± 1**	**<1**	**∼50**	Assessment [13]
		1805	7.5	0.8	48.3	Assessment [15]
		1781	7.3	0.5	49.0	This assessment

[a] The data printed in bold letters are those used for the optimisation.

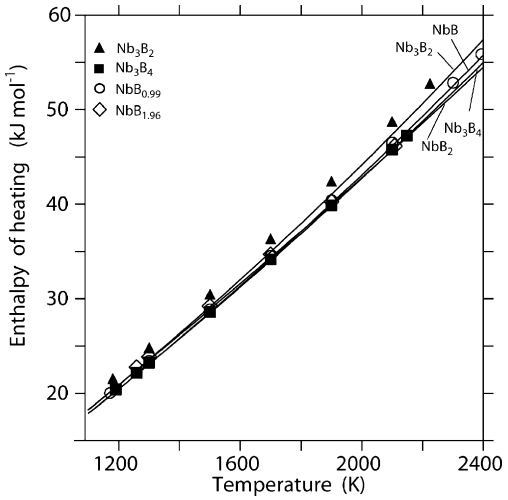

Fig. 2. Enthalpy change upon heating of niobium borides: points are experimental data of [38–40] and lines result from the present thermodynamic description.

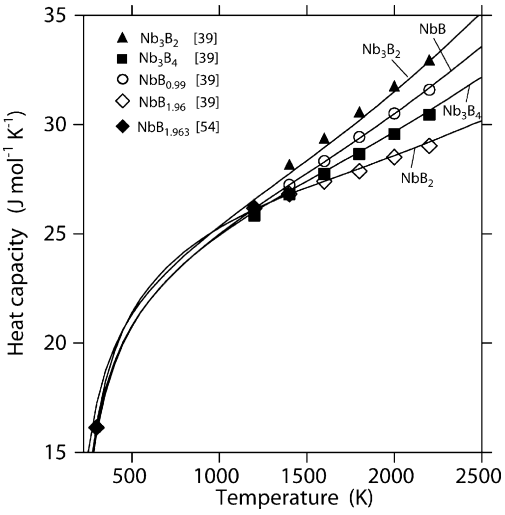

Fig. 3. Heat capacity of niobium borides: points are experimental data of [39,54] and lines result from the present thermodynamic description.

namic data. The obtained parameters were used as initial values in the further steps of optimisation.

The optimisation of the B–Nb phase diagram was continued in two steps. Firstly, the monoboride and the diboride of Nb were treated as stoichiometric compounds; in the second treatment they were treated by two-sublattice model, which are given in Sections 2.4 and 3.3. The parameters obtained from the previous treatments were used as starting values for the following action.

In the B–Ti system the parameters obtained in prior description by Ma et al. [15], exempting those for the monoboride and diboride of Ti, were used as starting values.

5. Results and discussion

The excess Gibbs energy coefficients for the phases of the B–Nb and B–Ti systems are summarised in Tables 3 and 4, respectively. The evaluated sets of the parameters were used to calculate phase diagrams and thermodynamic properties of the phases of these binary systems using the computer program Thermo-Calc [20].

5.1. The binary system B–Nb

Comparison between calculated and experimental values [38–40,54] for enthalpy change upon heating and heat capacity are shown in Figs. 2 and 3, respectively. Obviously, the agreement is excellent. Fig. 4 illustrates the composition dependency of the standard enthalpy of formation of solid phases at 298 K as well as the enthalpy of mixing for the liquid phase at 3500 K, as calculated with the optimised thermodynamic dataset. Here the experimental data, for the exception of the diboride, are scarce. The calculated curve for the standard enthalpy of formation of solid phases matches well with the data of [41,42,44].

A comparison between the calculated B–Nb phase diagram and experimental phase diagram data is illustrated in Fig. 5. It can be seen that the present description reproduces the invariant equilibria and the experimental data of [27,29,30,32,35,37], as well as the data on isothermal melting and incipient melting by DTA from [22], quite well. It should be mentioned that the temperatures at which the sample collapsed do not relate to liquidus temperatures (see also B–Ti [12,22] and B–Hf [55] systems). Table 5 summarises the invariant reactions in the B–Nb system, both calculated and experimentally determined.

5.2. The binary system B–Ti

The thermodynamic functions calculated according to the parameters presented in Table 4 are compared with experimental data for the B–Ti system as shown in Figs. 6–8. It can be seen that the calculated heat capacity of the diboride TiB_2 (see Fig. 6) is well compatible with experimental results. It should

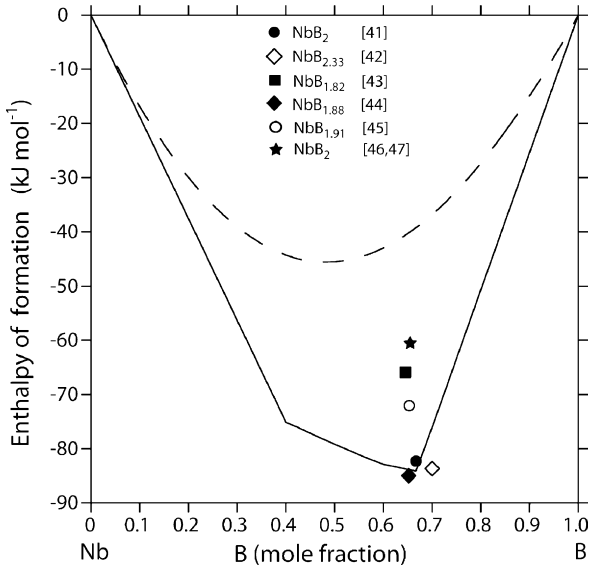

Fig. 4. Enthalpy of formation of the liquid phase at 3500 K (reference state is liquid components; dashed line) and of solid phases at 298 K (reference state is bcc-Nb and β-B; solid line) in the binary system B–Nb: points are experimental data for borides [41–47] and lines result from the present thermodynamic description. The data of Refs. [43,45–47] were not used for the optimisation.

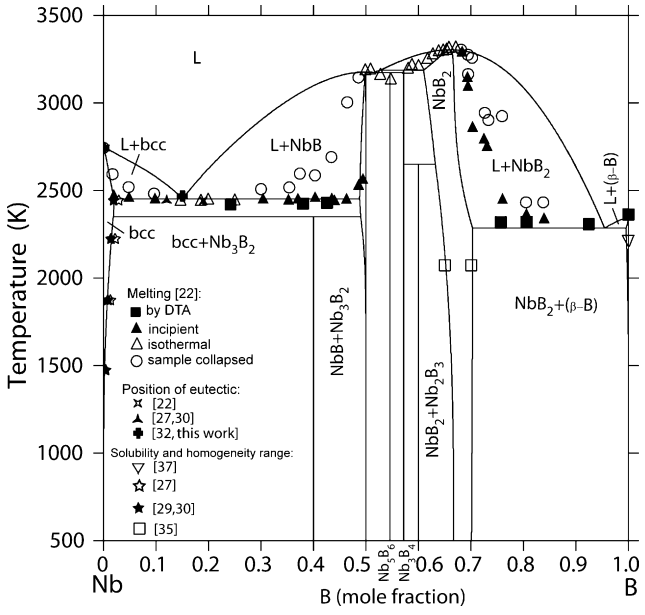

Fig. 5. Phase diagram of the system B–Nb: points are experimental data of [22,27,29,30,32,35,37] and lines result from the present thermodynamic description.

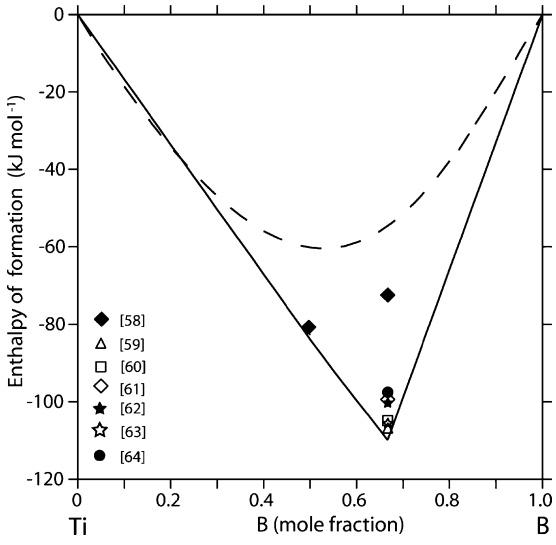

Fig. 7. Enthalpy of formation of the liquid phase at 3500 K (dashed line) and of solid phases at 298 K (solid line) in the binary system B–Ti: points are experimental data for borides [58–64] and lines result from the present thermodynamic description. Data for the diboride of Refs. [58,61,62,64] were not used in the optimisation.

be underlined that the estimated values of the heat capacity for the TiB monoboride that were based on analogy to monoborides from other B–M systems by [56] (marked as triangles in Fig. 6) are unreliable and were not used in the optimisation.

The calculated standard enthalpy of formation of solid phases at 298 K (see Fig. 7) and the calculated entropy at 298 K (see Fig. 8) as function of composition reproduce the majority of the experimental data available.

The comparison of the calculated phase diagram of the B–Ti system with experimental data is shown in Fig. 9. Obviously, the present description fits well to the experimental results of the present work, as well as to the data from [22,50,51,53]. Comparison of the calculated invariant reactions in the system with experimental data is listed in Table 6.

Finally, the calculation of the metastable invariant reaction $L + TiB_2 \leftrightarrow TiB$ performed using the present description gave the temperature 2400 K and composition of liquid equal to Ti–31.0 at.% B. It is highly probably that just this reaction temperature was determined in some works rather than a temperature for the reactions with the participation of Ti_3B_4 ($L + Ti_3B_4 \leftrightarrow TiB$ or $L + TiB_2 \leftrightarrow Ti_3B_4$) as was claimed.

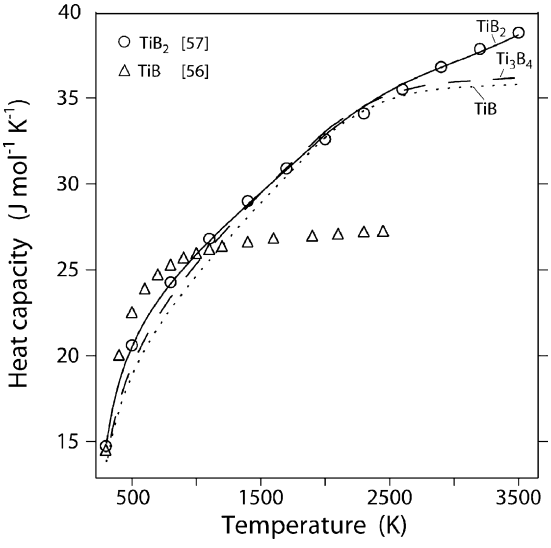

Fig. 6. Heat capacity of borides in the Ti–B system: lines are calculated data using the present thermodynamic description; circles are experimental data of [57] for the TiB_2; triangles are estimated data of [56] for the TiB (these data were not used in the optimisation).

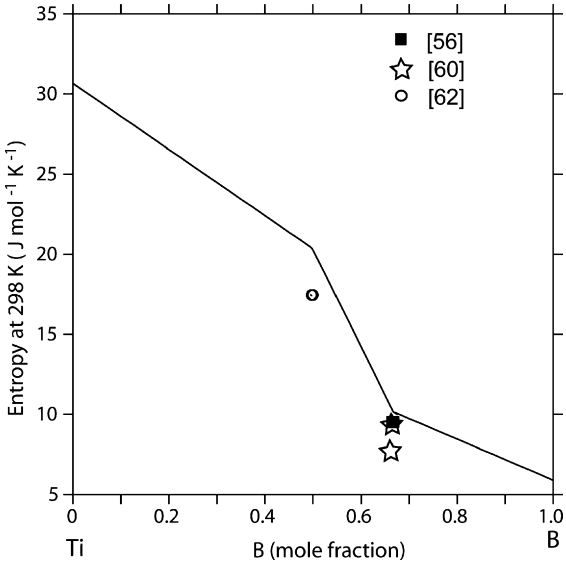

Fig. 8. Entropy at 298 K for the solid phases of the binary system B–Ti: points are evaluated data using the second and third thermodynamic law [56,60,62] and the line results from the present thermodynamic description.

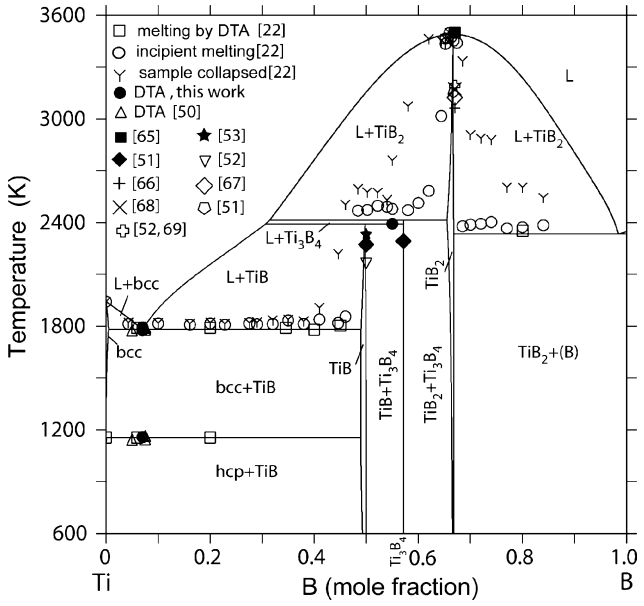

Fig. 9. Phase diagram of the system B–Ti: points are experimental data of [22,32,50–53,65–69] as well as DTA results of this work and lines result from the present thermodynamic description.

6. Summary and conclusions

In the present work, the thermodynamic descriptions of the binary systems B–Nb and B–Ti have been elaborated, involving:

- Critical assessment of phase equilibria in the system B–Nb.
- Key experiments for the determination of the temperature of the invariant reactions $L \leftrightarrow \mathrm{bcc} + \mathrm{NbB}$, $L \leftrightarrow \mathrm{bcc} + \mathrm{TiB}$, $L + \mathrm{Ti_3B_4} \leftrightarrow \mathrm{TiB}$ and $L + \mathrm{TiB_2} \leftrightarrow \mathrm{Ti_3B_4}$.
- Thermodynamic descriptions of the B–Nb and B–Ti systems based on critically assessed experimental values for phase equilibria and thermodynamic data.
- Thermodynamic equilibrium calculations of thermodynamic properties and phase diagrams in comparison to experimental data from various sources.

The proposed thermodynamic descriptions for the B–Nb and B–Ti systems match well to experimentally determined phase equilibria and selected thermodynamic properties. The advantages of these descriptions relates to their good integration into high-order systems Al–B–Ti and B–Nb–Ti, which will be discussed in the next parts of this work.

Acknowledgements

The authors from ACCESS e.V. would like to express their gratitude for financial support from Integrated Project IMPRESS, “Intermetallic Materials Processing in Relation to Earth and Space Solidification” (Contract NMP3-CT-2004-500635) co-funded by the European Commission in the Sixth Framework Programme, the European Space Agency and the Swiss Government.

The authors from IPMS appreciate financial supports of the Air Force Office of Scientific Research (USA) under the STCU Project P-060 (the B–Ti system) and the Ukrainian Government under the NASU Project 0103U005196 (the B–Nb system).

References

[1] F. Appel, M. Oehring, R. Wagner, Intermetallics 8 (2000) 1283–1312.
[2] S.C. Huang, in: R. Darolia, L. Lewandowski, C.T. Liu, P. Martin, D. Miracle, M. Nathal (Eds.), Structural Intermetallics, TSM, Warrendale, PA, 1993, p. 299.
[3] D.M. Dimiduk, in: Y.-K. Kim, R. Wagner, M. Yamagushi (Eds.), Gamma Titanium Aluminides, TSM, Warrendale, PA, 1995, p. 21.
[4] W.J. Zhang, F. Appel, Mater. Sci. Eng. A 329–331 (2002) 649–652.
[5] M.E. Hyman, C. McCullough, J.J. Valencia, C.G. Levi, R. Mehrabian, Metall. Trans. 20A (1989) 1847.
[6] J.A. Christodoulou, H.M. Flower, Adv. Eng. Mater. 2 (2000) 631.
[7] B.J. Inkson, C.B. Boothroyd, C.J. Humphreys, J. Phys. IV 3 (1993) 397–402.
[8] T.T. Cheng, Intermetallics 8 (2000) 29–37.
[9] P.J. Maziasz, R.V. Ramanujan, C.T. Liu, J.L. Wright, Intermetallics 5 (1996) 83.
[10] D.J. Larson, C.T. Liu, M.K. Miller, Intermetallics 5 (1997) 411–414.
[11] U. Kitkamthorn, L.C. Zhang, M. Aindow, Intermetallics 14 (2006) 759–769.
[12] L. Kaufman, B. Uhrenius, D. Birnie, K. Taylor, Calphad 8 (1984) 25–66.
[13] J.L. Murray, P.K. Liao, K.E. Spear, in: J.L. Murray (Ed.), Phase Diagrams of Binary Titanium Alloys, ASM International, Metals Park, OH, 1987.
[14] C. Bätzner, in: I. Ansara, A.T. Dinsdale, M.H. Rand (Eds.), Thermodynamic Database for Light Metal Alloys, European Commission, Luxemburg, 1998.
[15] X. Ma, C. Li, Z. Du, W. Zhang, J. Alloys Compd. 370 (2004) 149–158.
[16] A.T. Dinsdale, Calphad 15 (1991) 317–425.
[17] O. Redlich, A.T. Kister, Ind. Eng. Chem. 40 (1948) 345–348.
[18] M. Hillert, L.-I. Staffansson, Acta Chem. Scand. 24 (1970) 3618–3626.
[19] B. Sundman, J. Ågren, J. Phys. Chem. Solids 42 (1981) 297–301.
[20] B. Sundman, B. Jansson, J.-O. Andersson, Calphad 9 (1985) 153–190.
[21] C. Servant, I. Ansara, Ber. Bunsenges. Phys. Chem. 102 (1998) 1189–1205.
[22] E. Rudy, Ternary Phase Equilibria in Transition Metal–Boron–Carbon–Silicon Systems. Part V. Compendium of Phase Diagram Data, Tech. Rep. AFML-TR-65-2, Part V, Air Force Materials Laboratory, Wright-Patterson AFB, OH, 1969.
[23] P. Rogl, in: P. Rogl, J.C. Schuster (Eds.), Phase Diagrams of Ternary Boron Nitride and Silicon Nitride Systems, ASM, Materials Park, OH, 1992, pp. 68–72.
[24] P. Rogl, in: G. Effenberg (Ed.), Phase Diagrams of Metal–Boron–Carbon Ternary Systems, ASM-MSI, Materials Park, OH, 1998, pp. 202–205.
[25] N.P. Lyakishev (Ed.), Phase Diagrams of Binary Metal Systems, vol. 1, Mashinostriyeniye, Moscow, 1996, pp. 465–467 (in Russian).
[26] T.V. Massalski, P.R. Subramanian, H. Okomoto, L. Kasprzak (Eds.), Binary Alloy Phase Diagrams, vol. 3, 2nd ed., ASM International, Materials Park, OH, 1990.
[27] V.P. Pshokin, A.M. Zakharov, Izv. VUZov, Tsvetnaya Metallurg. (1) (1971) 111–114 (in Russian).
[28] H. Nowotny, F. Benesovsky, R. Kieffer, Z. Metallkd. 50 (1959) 417–423.
[29] A.M. Zakharov, V.P. Pshokin, E.I. Ivaniva, Izv. AN SSSR, Met. (5) (1985) 193–196 (in Russian).
[30] A.M. Zakharov, V.P. Pshokin, Izv. AN SSSR, Met. (6) (1985) 195–196 (in Russian).
[31] L.A. Borges Jr., G.C. Coelho, C.A. Nunes, P.A. Suzuki, J. Phase Equilib. 24 (2003) 140–146.
[32] D.B. Borysov, L.V. Artyukh, A.A. Bondar, P.S. Martsenyuk, A.V. Samelyuk, N.I. Tsyganenko, O.S. Fomichov, T.Ya. Velikanova, Poroshkovaya Metallurgiya (Powder Metall. Met. Ceram.), in press.
[33] H. Bolmgren, T. Lundström, J. Less-Common Met. 159 (1990) L25–L27.
[34] C.A. Nunes, B.B. de Lima, G.C. Coelho, P. Rogl, P.A. Suzuki, J. Less-Common Met. 370 (2004) 164–168.

[35] C.A. Nunes, D. Kaczorowski, P. Rogl, M.R. Baldissera, P.A. Suzuki, G.C. Coelho, A. Grytsiv, G. Andre, F. Bourree, S. Okada, Acta Mater. 53 (2005) 3679–3687.
[36] S. Okada, K. Hamano, T. Lundström, I. Higashi, in: D. Emin, T.L. Aselage, A.C. Switendick, G.B. Morosiz, C.L. Beckel (Eds.), AIP Conf. Proc. 231 "Boron-Rich Solid" (10th International Symposium on Boron, Borides and Related Compounds, 1990, Albuquergue, NM, USA), AIP, New York, 1991, pp. 456–459.
[37] A.J. Crespo, L.E. Tergenius, T. Lundström, J. Less-Common Met. 77 (1981) 147–150.
[38] A.S. Bolgar, M.I. Serbova, T.I. Serebryakova, L.F. Isaeva, V.V. Fesenko, Poroshkovaya Metallurgiya (3) (1983) 57–62, Engl. transl.: Soviet Powder Met. Ceram. 22 (3) (1983) 207–211.
[39] A.S. Bolgar, A.B. Lyashenko, L.A. Klochkov, A.V. Blinder, A.V. Muratov, J. Less-Common Met. 117 (1986) 303–306.
[40] A.V. Blinder, A.S. Bolgar, Poroshkovaya Metallurgiya (12) (1991) 72–76, Engl. transl.: Soviet Powder Met. Ceram. 30 (12) (1991) 1053–1056.
[41] G.V. Samsonov, Russ. J. Phys. Chem. 30 (1956) 2057.
[42] L. Kaufman, in: J. Waber (Ed.), Compounds of Interest in Nuclear Reactor Technology, vol. 7, AIME, 1964, p. 193.
[43] L.A. Reznitskii, Russ. J. Phys. Chem. 41 (1967) 612–614.
[44] G.K. Johnson, E. Greenberg, J.L. Margrave, W.N. Hubbard, J. Chem. Eng. Data 12 (1967) 597–600.
[45] E.P. Kirpipichev, Yu.I. Rubtsov, T.V. Sorokina, V.K. Prokudina, Russ. J. Phys. Chem. 53 (1979) 1980–1983.
[46] S.V. Meschel, O.J. Kleppa, Metall. Trans. 24A (1993) 947–950.
[47] S.V. Meschel, O.J. Kleppa, J. Alloys Compd. 321 (2001) 183–200.
[48] P. Villars, L.D. Calvert, Pearson's Handbook of Crystallographic Data for Intermetallic Phases, vol. 4, 2nd ed., ASM, Metals Park, OH, 1991.
[49] J. Thebault, R. Pailler, G. Bontemps-Moley, M. Bourdeau, R. Naslain, J. Less-Common Met. 47 (1976) 221–233.
[50] A.A. Bondar, L.V. Artyukh, T.Ya. Velikanova, O.O. Bilous, M.P. Burka, O.S. Fomichov, N.I. Tsyganenko, S.O. Firstov, Intermetallics, in press.
[51] R.G. Fenish, Phase Relationships in the Titanium–Boron System, NRM-138, 1964, pp. 1–37.
[52] P. Schwarzkopf, F.W. Glaser, Z. Metallkd. 44 (1953) 353–358 (in German).
[53] A.E. Palty, H. Margolin, J.P. Nielsen, Trans. ASM 46 (1954) 312–328.
[54] E.F. Westrum, G.A. Glay, J. Phys. Chem. 67 (1963) 2385–2387.
[55] H. Bittermann, P. Rogl, J. Phase Equilib. 18 (1997) 24–46.
[56] M.W. Chase, NIST-JANAF Thermochemical Tables, 4th ed., American Institute of Physics for the National Institute of Standards and Technology, 1998.
[57] D.R. Stull, H. Prophet, JANAF Thermochemical Tables, 2nd ed., Nat. Stand. Ref. Data Ser., Nat. Bur. Stand, US, 1971.
[58] P.O. Schissel, W.S. Williams, Bull. Am. Phys. Soc. Ser. II 4 (1959) 189.
[59] L. Guzman, M. Elena, A. Miotello, P.M. Ossi, Vacuum 46 (1995) 951–954.
[60] T.J. Yurick, K.E. Spear, Thermodyn. Nucl. Mater., 1979, vol. I, IAEA-SM-236/532, Vienna (1980) 73–90.
[61] L. Brewer, H. Haraldsen, J. Electrochem. Soc. 102 (1955) 349–406.
[62] P. Schissel, O. Trulson, J. Phys. Chem. 66 (1962) 1492–1496.
[63] V.V. Akhachinskij, N.A. Chirin, Thermodyn. Nucl. Mater., 1974, vol. II, IAEC, Vienna (1975) 467–476.
[64] W. Williams, J. Phys. Chem. 65 (1961) 2213–2216.
[65] H. Holleck, J. Vac, Sci. Technol. A 4 (6) (1986) 2661–2669.
[66] F.W. Glaser, Trans. AIME 194 (1952) 391–396.
[67] I.I. Lskoldsky, L.R. Bogorodskaya, Zh. Prikl. Khim. 30 (1957) 177–185 (in Russian).
[68] R. Kieffer, F. Benesovsky, E.R. Honak, Z. Anorg. Chem. 268 (1952) 191–200.
[69] B. Post, F.W. Glaser, D. Moskowitz, Acta Metall. 2 (1954) 20–25.
[70] H.R. Ogden, R.I. Jaffee, Trans. AIME 191 (1951) 335–336.